Highly-Efficient, Compact Tm^{3+}:RE_2O_3 (RE = Y, Lu, Sc) Sesquioxide Lasers Based on Thermal Guiding

Pavel Loiko, Philipp Koopmann, Xavier Mateos, Josep Maria Serres, Venkatesan Jambunathan, Antonio Lucianetti, Tomas Mocek, Magdalena Aguiló, Francesc Díaz, Uwe Griebner, Valentin Petrov, and Christian Kränkel

***Abstract*— Cubic sesquioxides, RE_2O_3, where RE = Y, Lu or Sc, are attractive host crystals for thulium (Tm^{3+}) doping. A comparison of the spectroscopic properties of Tm^{3+}:RE_2O_3 crystals in terms of transition cross-sections and cross-relaxation (CR) efficiency required for efficient upconversion pumping is presented. Thermo-optic properties of Tm^{3+}:RE_2O_3 crystals (thermal lensing, fractional heat loading and thermo-optic coefficients) are described. The positive thermal lens, broadband emission and efficient CR of the Tm:RE_2O_3 crystals enable the development of compact, highly-efficient and power-scalable lasers operating above 2 µm, based on thermal guiding. Nowadays, Tm:Lu_2O_3 microchip lasers are capable of generating nearly 5 W of output power at ~2.06 µm with a slope efficiency η of 67% and in a rod geometry - up to 47.5 W with η of 59%. For multi-watt output at even longer wavelengths around 2.15 µm, Tm:Sc_2O_3 is an interesting candidate.**

***Index Terms*— Solid-state lasers, sesquioxide crystals, thulium doping, thermal lensing.**

I. Introduction

Rare-earth (RE) sesquioxides, RE_2O_3, represent a well-known family of crystals. Depending on the RE element and the growth conditions, there exist several structural modifications: hexagonal (A-type, for RE = La…Nd), monoclinic (B-type, for RE = Sm, Eu, Gd) or cubic (C-type, for RE = Sm...Lu, Sc, and Y). In particular the last one, or the bixbyite structure (the mineral bixbyite, $(Mn,Fe)_2O_3$, possesses the space group $Ia\bar{3}$) [1], is attractive for laser applications [2]. The cubic crystals of Lu_2O_3 (Lutetia), Sc_2O_3 (Scandia), and Y_2O_3 (Yttria) have been recognized as excellent host matrices for doping with laser-active RE^{3+} ions, such as Yb^{3+} [3,4], Tm^{3+} [5,6], Ho^{3+} [7,8], Nd^{3+} [9] or Er^{3+} [10]. These crystals will be referred in this paper as "cubic sesquioxides". It should be noted that there also exist cubic "mixed" sesquioxide crystals. Any solid solution of the above 3 obviously will exhibit cubic structure, e.g. $(Lu,Sc)_2O_3$ [11].

The interest in RE^{3+}-doped cubic sesquioxides is mostly due to their superior thermal properties and spectroscopic features. The RE_2O_3 crystals possess high thermal conductivity (12.8 W/mK for undoped Lu_2O_3, higher than that of YAG) with weaker dependence on the RE^{3+} doping level [6,12], and weak thermal expansion [13,14]. These crystals have high melting temperature (2450 °C for Lu_2O_3 [15]), underlying good mechanical and chemical stability, and wide band-gaps. The cubic sesquioxides exhibit a broad transparency range (0.22 – 8 µm) [2] and moderate maximum phonon frequency for oxide materials [16].

There are two crystallographic sites in the bixbyite structure that can be occupied by the RE^{3+} dopant ions (C_2 and C_{3i} symmetry, 24*d* and 8*b* Wyckoff positions, respectively) [17] but the optical properties are largely determined by doping ions on C_2-sites [2]. This is because for the C_{3i} site, the electric-dipole transitions are forbidden due to inversion symmetry. For both sites, the RE^{3+} ions have a VI-fold O^{2-} coordination. This coordination is lower than e.g. for RE^{3+} in YAG and features short RE^{3+}-O^{2-} distances leading to a strong crystal field and correspondingly broad absorption and emission spectral bands [2]. The latter enables very broad laser wavelength tuning ranges [18,19] and the generation of ultrashort pulses in the mode-locked (ML) regime [20-24]. Due to the good thermal properties of the host, power-scaling of bulk and thin-disk continuous-wave (CW) [12,18] and ML [25-28] sesquioxide lasers is feasible.

Manuscript received September X, 2017. This work was supported by the Spanish Government under projects MAT2016-75716-C2-1-R, (AEI/FEDER, UE), TEC 2014-55948-R, and by the Generalitat de Catalunya under project 2014SGR1358. F.D. acknowledges additional support through the ICREA academia award 2010ICREA-02 for excellence in research. P.L. acknowledges financial support from the Government of the Russian Federation (Grant 074-U01) through ITMO Post-Doctoral Fellowship scheme.

P. Loiko is with ITMO University, Kronverkskiy pr., 49, Saint-Petersburg, 197101, Russia (e-mail: kinetic@tut.by).

P. Koopmann and C. Kränkel are with Institut für Laser-Physik, Universität Hamburg, Luruper Chaussee 149, D-22761 Hamburg, Germany (e-mail: pkoopman@physnet.uni-hamburg.de, kraenkel@physnet.uni-hamburg.de).

X. Mateos, J. M. Serres, M. Aguiló and F. Díaz are with Física i Cristal·lografia de Materials i Nanomaterials (FiCMA-FiCNA)-EMaS, Dept. Química Física i Inòrganica, Universitat Rovira i Virgili (URV), Campus Sescelades, E-43007 Tarragona, Spain (e-mail: xavier.mateos@urv.cat; jserrese@gmail.com; magdalena.aguilo@urv.cat, f.diaz@urv.cat).

V. Jambunathan, A. Lucianetti and T. Mocek are with HiLASE Centre, Institute of Physics of the Czech Academy of Sciences, Za Radnicí 828, 25241 Dolní Břežany, Czech Republic (e-mail: jambunath@fzu.cz, lucianetti@fzu.cz, mocek@fzu.cz).

U. Griebner and V. Petrov are with Max-Born-Institute for Nonlinear Optics and Short Pulse Spectroscopy, 2A Max-Born-Str., D-12489 Berlin, Germany (e-mail: griebner@mbi-berlin.de, petrov@mbi-berlin.de).

C. Kränkel is with Zentrum für Lasermaterialien - Kristalle (ZLM-K) at Leibniz-Institut für Kristallzüchtung (IKZ), 2 Max-Born-Str., 12489 Berlin, Germany (e-mail: christian.kraenkel@ikz-berlin.de)

The thulium (Tm^{3+}) ion (electronic configuration: [Xe]$4f^{12}$) is well-known for its eye-safe broadband emission at ~2 µm due to the $^3F_4 \rightarrow {}^3H_6$ transition [29], Fig. 1. Tm lasers are widely used in remote sensing, spectroscopy and medicine. They can be excited at ~0.8 µm (to the $^3H_4$ level) by commercial AlGaAs laser diodes. Moreover, an efficient cross-relaxation (CR) process for adjacent Tm^{3+} ions, $Tm_1(^3H_4) + Tm_2(^3H_6) \rightarrow Tm_1(^3F_4) + Tm_2(^3F_4)$ can lead to a quantum efficiency of 2 [31] resulting in weak heat load and allowing for a high slope efficiency despite the large energetic difference between pump and laser photons. Promising output characteristics have been demonstrated with $Tm:RE_2O_3$ crystals to date [5,6]. Owing to a large splitting of the ground-state multiplet, $^3H_6$, of the Tm^{3+} ion in RE_2O_3 (e.g. for Lu_2O_3: 792 cm^{-1}), laser emission at wavelengths >2 µm is possible [6,24] which is typically not the case for other well-known Tm^{3+}-doped laser materials, e.g. YAG or $LiYF_4$. Sub-200 fs pulses were achieved in the ML regime utilizing $Tm^{3+}:Lu_2O_3$ crystals [23].

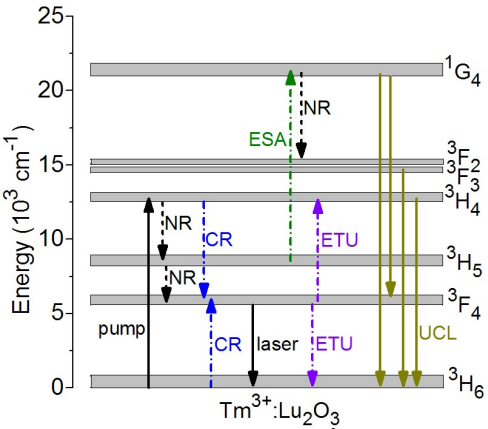

Fig. 1. Scheme of energy levels of the Tm^{3+} ion (on the example of $Tm^{3+}:Lu_2O_3$, C_2 site) showing relevant processes (CR – cross-relaxation, ETU – energy-transfer upconversion, ESA – excited-state absorption, UCL – upconversion luminescence, NR – non-radiative relaxation). The grey rectangles correspond to the total Stark splitting [30].

Tm^{3+}-doped sesquioxides have also been studied in the form of transparent ceramics. In particular, $Tm:Lu_2O_3$ ceramics have been employed in CW and ML bulk lasers [32,33].

The thermo-optic behavior of cubic $Tm:RE_2O_3$ crystals has not been addressed to date. However, this information is of key importance for the design of $Tm:RE_2O_3$ bulk and thin-disk lasers. In this work, we present a detailed comparative study of the thermo-optic effects in the three Tm^{3+}-doped cubic sesquioxides, Lu_2O_3, Y_2O_3 and Sc_2O_3 for wavelengths around 2 µm under lasing conditions. Moreover, we employ the measured positive thermal lens (TL) for thermal stabilization of the laser mode in compact plano-plano laser cavities [34] including the microchip design.

The microchip laser concept means an active element (AE) and (optionally) a saturable absorber (SA) for the passively Q-switched (PQS) operation placed in a compact plano-plano cavity without air gaps [35,36]. For a monolithic design, the cavity mirrors can be directly deposited on the optical surfaces of the AE (or SA). For a micro-laser design, all optical elements can be placed next to each other. Such compact, robust and low-loss laser design can provide high laser efficiency in CW regime and generation of short (down to sub-ns) pulses in PQS operation [36].

II. Spectroscopy of the Tm^{3+} Ion

Various 1.8 at.% Tm and 4.0 at.% $Tm:Lu_2O_3$ and 2.0 at.% $Tm:Sc_2O_3$ crystals were grown by the heat-exchanger method (HEM) [37] and a 2.5 at.% $Tm:Y_2O_3$ crystal by the Nacken-Kyropoulos (NK) method [5]. The corresponding calculated Tm^{3+} doping concentrations N_{Tm} are listed in Table I together with the measured crystal density ρ.

TABLE I
Studied Tm^{3+}-Doped Cubic Sesquioxide Crystals

Crystal	Doping	N_{Tm}, 10^{20} cm^{-3}	Growth method	ρ, g/cm^3
$Tm:Y_2O_3$	2.5 at.%	6.6	NK	5.01
$Tm:Lu_2O_3$	1.8 at.%	5.1	HEM	9.40
	4.0 at.%	11.2	HEM	9.33
$Tm:Sc_2O_3$	2.0 at.%	6.4	HEM	3.69

Prior to the presentation of the laser experiments, we compare the spectroscopic properties of Tm^{3+} in cubic Lu_2O_3, Y_2O_3 and Sc_2O_3 [30,38].

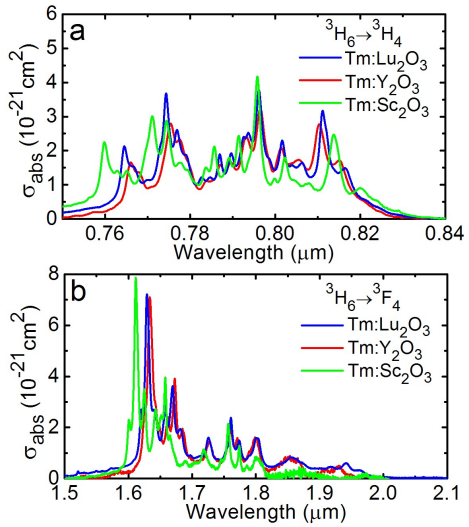

Fig. 2. Absorption cross-sections, σ_{abs}, for Tm^{3+} doped Lu_2O_3, Y_2O_3 and Sc_2O_3 for the (a) $^3H_6 \rightarrow {}^3H_4$ and (b) $^3H_6 \rightarrow {}^3F_4$ transitions [30,38].

A. Transition Cross-Sections

Figure 2(a) shows the absorption cross-sections, σ_{abs}, for the $^3H_6 \rightarrow {}^3H_4$ transition of Tm^{3+}. For all $Tm:RE_2O_3$ crystals, a broad and structured absorption band spanning from 0.76 to 0.83 µm is observed. The maximum σ_{abs} = 3.25, 3.77 and 4.19×10^{-21} cm^2 are found at 796.5, 796.2 and 795.8 nm for RE = Y, Lu and Sc, respectively. The full width at half maximum (FWHM) of the corresponding absorption peaks amounts to 7.1, 6.2 and 2.4 nm, respectively. The absorption cross-section spectra for the $^3H_6 \rightarrow {}^3F_4$ transition are shown in Fig. 2(b).

The Stark splitting of the lower and upper laser levels, $^3H_6$ and $^3F_4$, of Tm^{3+} in cubic Y_2O_3, Lu_2O_3 and Sc_2O_3 crystals (for the C_2 sites) is shown in Fig. 3. The crystal field strength tends to increase with decreasing cation radius r. Therefore, the Stark splitting of both multiplets increases from Y^{3+} (r_Y = 0.90 Å, $\Delta E(^3H_6)$ = 792 cm^{-1}) via Lu^{3+} (r_{Lu} = 0.861 Å, $\Delta E(^3H_6)$ = 892 cm^{-1}) to Sc^{3+} (r_{Sc} = 0.745 Å, $\Delta E(^3H_6)$ = 955 cm^{-1}). In contrast, the

energy of the transitions between the lowest Stark sub-levels of the two multiplets is nearly identical and at ~5610 cm^{-1}, giving rise to pure electronic transitions at wavelengths between 1.8 μm and up to 2.15 μm in Sc_2O_3.

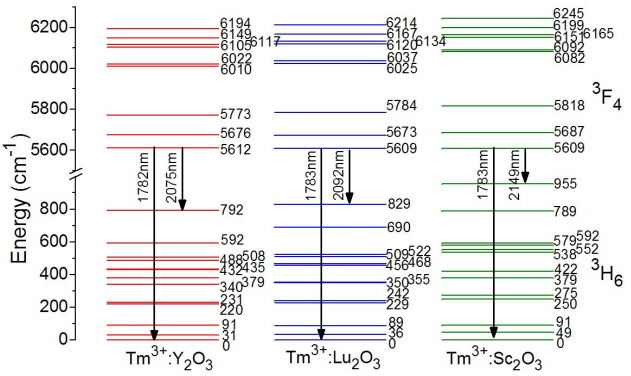

Fig. 3. Stark splitting of the ground-state, $^3H_6$, and the upper laser level, $^3F_4$, for Tm^{3+} in cubic Y_2O_3, Lu_2O_3 and Sc_2O_3 (C_2 sites) [30,38]. *Numbers* are the energies of Stark sub-levels in wavenumbers (cm^{-1}), *arrows* indicate the electronic transitions between the lowest Stark sub-levels of the two multiplets and the one corresponding to the longest wavelength.

The stimulated-emission (SE) cross-sections σ_{SE} for the $^3F_4 \rightarrow {}^3H_6$ transition calculated with the Füchtbauer-Ladenburg equation [39] are presented in Fig 4. The maximum σ_{SE} are 8.8, 10.7 and 10.2×10^{-21} cm^2 at 1933, 1943 and 1972 nm for Tm^{3+} doped Y_2O_3, Lu_2O_3 and Sc_2O_3, respectively.

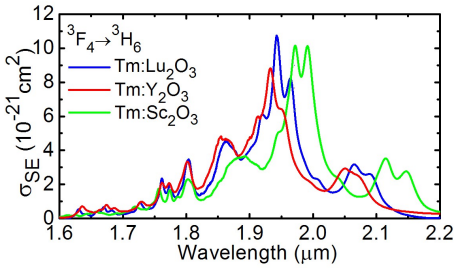

Fig. 4. Stimulated-emission (SE) cross-sections, σ_{SE}, for the $^3F_4 \rightarrow {}^3H_6$ transition of Tm^{3+} in cubic Lu_2O_3, Y_2O_3 and Sc_2O_3 [30,38].

Tm^{3+} represents a quasi-three-level laser scheme. To conclude about expected laser wavelengths, the gain cross-sections, $\sigma_g = \beta\sigma_{SE} - (1-\beta)\sigma_{abs}$, where $\beta = N(^3F_4)/N_{Tm}$ is the inversion ratio, are typically calculated. The gain spectra for Tm:RE_2O_3 crystals are shown in Fig. 5(a-c). For Tm:Lu_2O_3, at small inversion ratios ($\beta < 0.06$), the laser operation is expected at wavelengths beyond 2 μm (at 2066 and 2093 nm) and for higher β, the maximum shifts to shorter wavelengths around 1965 and 1933 nm. A similar behavior is observed for Tm:Y_2O_3 and Tm:Sc_2O_3. The position of all local peaks in the gain spectra is red-shifted in the sequence RE = Y – Lu – Sc.

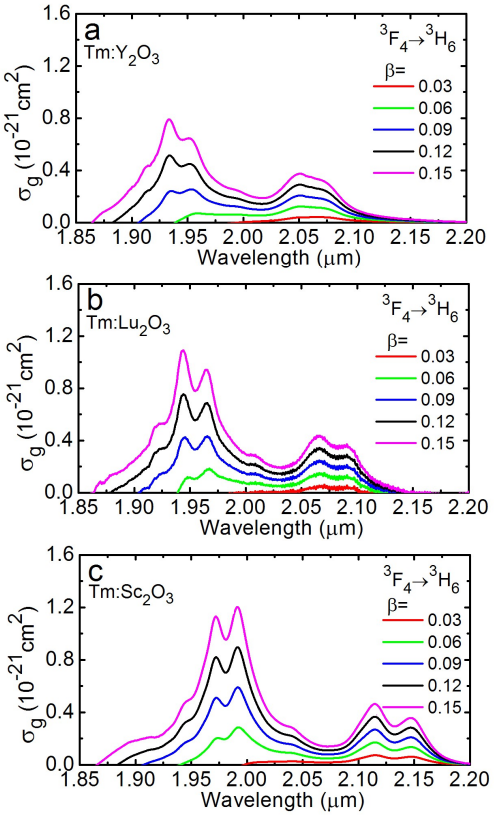

Fig. 5. Gain cross-sections, $\sigma_g = \beta\sigma_{SE} - (1-\beta)\sigma_{abs}$, for (a) Tm:$Y_2O_3$, (b) Tm:$Lu_2O_3$ and (c) Tm:Sc_2O_3 crystals, $\beta = N(^3F_4)/N_{Tm}$ is the inversion ratio.

B. Emission Lifetimes and Cross-Relaxation

Table II shows a comparison of calculated radiative lifetimes, τ_{rad}, and measured luminescence lifetimes, τ_{lum}, of the upper-laser-level ($^3F_4$) of Tm^{3+} in cubic sesquioxides [30,38]. Here, τ_{rad} was determined with the standard Judd-Ofelt (J-O) theory (the corresponding J-O (intensity) parameters are also listed in Table II) or estimated from the integrated σ_{SE} spectra [38]. The luminescence lifetime of the emitting level $^3F_4$ for cubic Tm:RE_2O_3 crystals is ~3.5 ms and it is only slightly shorter than the radiative one. This is due to weak non-radiative (NR) relaxation for these hosts determined by the relatively low maximum phonon frequency, $h\nu_{ph}$ = 592, 612 and 669 cm^{-1} for RE = Y, Lu and Sc, respectively [16,40].

Quantification of CR in Tm^{3+}-doped materials is based on the analysis of the luminescence lifetime of the $^3H_4$ pump level which is shortened with increasing doping concentration N_{Tm} according to [31]:

$$1/\tau_{lum}(^3H_4) = 1/\tau_{lum0}(^3H_4) + C_{CR}N_{Tm}^2. \qquad (1)$$

Here, C_{CR} is the microscopic concentration-independent CR parameter and τ_{lum0} is the intrinsic luminescence lifetime of the $^3H_4$ state (in the absence of CR). The quantum efficiency of the excitation of Tm^{3+} ions, i.e., the number of emitted photons at ~2 μm per one pump photon, η_q is then [31,41]:

$$\eta_q = 1 + \frac{C_{CR}N_{Tm}^2}{1/\tau_{lum0}(^3H_4) + C_{CR}N_{Tm}^2}, \qquad (2)$$

so that $1 \le \eta_q \le 2$. Eq. (2) is derived under the assumption of weak ground-state ($^3H_6$) bleaching and the lack of parasitic processes, energy-transfer upconversion (ETU), e.g. $Tm_1(^3F_4) + Tm_2(^3F_4) \rightarrow Tm_1(^3H_4) + Tm_2(^3H_6)$, and excited-state absorption (ESA), $^3H_5 \rightarrow {}^1G_4$, see Fig. 1.

TABLE II
JUDD-OFELT PARAMETERS AND UPPER-LASER-LEVEL LIFETIMES OF Tm^{3+} IONS IN CUBIC SESQUIOXIDES [30,38]

Crystal	Ω_k, 10^{-20} cm^2			$\tau_{rad}(^3F_4)$, ms		$\tau_{lum}(^3F_4)$*, ms
	Ω_2	Ω_4	Ω_6	J-O	Int. σ_{SE}**	
$Tm:Y_2O_3$	3.169	1.433	0.482	4.98	4.00	3.54
$Tm:Lu_2O_3$	2.874	1.384	0.456	5.22	3.79	3.38
$Tm:Sc_2O_3$	2.577	0.879	0.669	6.12	4.59	3.57

*Measured for crystals with <0.3 at.% Tm^{3+} doping.
**Estimated from the integrated σ_{SE} spectrum.

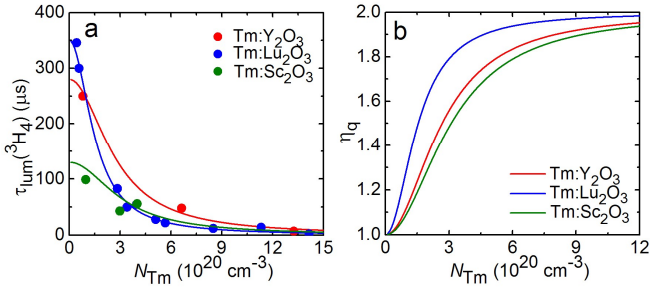

Fig. 6. (a) Luminescence lifetimes of the $^3H_4$ state of Tm^{3+} in cubic RE_2O_3 crystals (*symbols* – experimental data [30,38], *curves* – their fitting by Eq. (1)); (b) calculated quantum efficiency of the excitation of Tm^{3+} ions η_q for the cubic $Tm:RE_2O_3$ crystals *vs.* N_{Tm}.

TABLE III
PARAMETERS OF CROSS-RELAXATION IN Tm^{3+}-DOPED CUBIC SESQUIOXIDES

Crystal	$\tau_{rad}(^3F_4)$ [38], μs [38]	$\tau_{lum0}(^3F_4)$, μs	C_{CR}, 10^{-37} cm^6/s	η_q* (Tm doping)
$Tm:Y_2O_3$	670	280	0.5±0.1	1.86 (2.5 at.%)
$Tm:Lu_2O_3$	690	350	1.25±0.05	1.91 (1.8 at.%)
$Tm:Sc_2O_3$	640	130	0.8±0.1	1.81 (2.0 at.%)

*Calculated with Eq. (2).

In Fig. 6(a), we have plotted the reported [30,38] values of $\tau_{lum}(^3F_4)$ for cubic $Tm:RE_2O_3$ crystals with different Tm^{3+} concentrations. These points were fitted by Eq. (1) to extract $\tau_{lum0}(^3F_4)$ and C_{CR}, see Table III where the radiative lifetimes of the $^3H_4$ state determined with the J-O theory are also shown. For $Tm:Lu_2O_3$, $\tau_{lum0}(^3F_4) = 350$ μs and $C_{CR} = (1.25\pm0.05) \times 10^{-37}$ cm^6/s, cf. with $Tm:KLu(WO_4)_2$, a well-known crystal featuring efficient cross relaxation, $\tau_{lum0}(^3F_4) = 240$ μs and $C_{CR} = 2.7\times10^{-37}$ cm^6/s [42]. For the same N_{Tm}, the cross relaxation efficiency decreases in the sequence RE = Lu – Y – Sc. For 1.8 at.% Tm^{3+} doping, the value of η_q calculated with Eq. (2) reaches 1.91 for $Tm:Lu_2O_3$ and it is slightly lower, $\eta_q = 1.86$ for 2.5 at.% $Tm:Y_2O_3$ and 1.81 for 2 at.% $Tm:Sc_2O_3$. Thus, the doping concentrations selected for the laser experiments (cf. Table I) are adequate for efficient cross relaxation.

III. THERMO-OPTICAL PROPERTIES

A. Thermal Lensing

Thermal lensing was studied in 2.5 at.% $Tm:Y_2O_3$, 1.8 at.% $Tm:Lu_2O_3$ and 2.0 at.% $Tm:Sc_2O_3$ crystals by analyzing the divergence of the laser beam with the ABCD formalism. The dimensions of the studied crystals were the same as specified in Section IV A. A hemispherical laser cavity with the laser operating in TEM_{00} mode was used, see Fig. 7. The thermal lens (TL) was considered as an ideal thin lens located close to the input face of the active element. This method allowed us to study the TL under lasing conditions at the laser wavelength λ_L. More details can be found elsewhere [43].

The $Tm:RE_2O_3$ crystals were mounted in a Cu-holder, water-cooled to 12 °C, using indium foil to improve the thermal contact with all 4 lateral sides. The laser cavity consisted of a flat pump mirror (PM) with high transmission (HT) at 0.8 μm and high reflection (HR) at 1.8-2.1 μm, and a concave output coupler (OC) with a radius of curvature of 50 mm and a transmission of $T_{OC} = 3\%$ at 1.8-2.1 μm. In the cavity with a geometrical length L_{cav} of 49 mm the crystal was placed at a distance of 1 mm from the pump mirror. It was pumped by a fiber-coupled (fiber core diameter: 200 μm, numerical aperture, N.A.: 0.22) AlGaAs laser diode which emitted up to 25 W of unpolarized output at $\lambda_p = 802$ nm (diode #1); the emission wavelength was controlled by water-cooling. The pump radiation was collimated and focused into the crystal through the pump mirror by a lens assembly (imaging ratio: 1:1, focal length: 30 mm) resulting in a pump spot radius w_p of 100 μm in the focus and a confocal parameter $2z_R$ of 1.73 mm (in the crystal). The position of the pump waist was adjusted for each crystal until a TEM_{00} output mode was observed. The radius of the output laser beam was measured at 26 cm from the OC by the optical knife edge method (according to the ISO 11146-1-2005 standard).

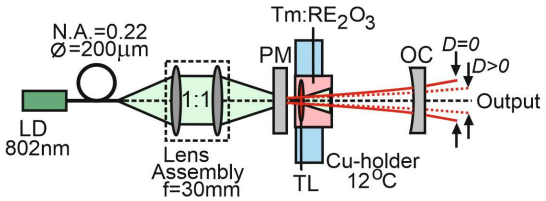

Fig. 7. Scheme of the $Tm:RE_2O_3$ laser used for the thermal lens (TL) measurements: LD – laser diode, PM – pump mirror, OC – output coupler.

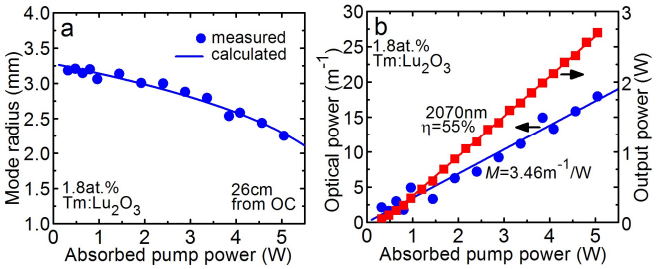

Fig. 8. Measurement of the TL in a 1.8 at.% $Tm:Lu_2O_3$ crystal: (a) radius of the output laser mode measured at 26 cm from the OC (*circles* – experimental data, *curve* – ABCD-modelling); (b) calculated optical (refractive) power of the TL (*circles* – experimental data, *line* – linear fit for the determination of the sensitivity factor, M) and the corresponding input-output dependence of the laser, η – slope efficiency ($\lambda_p = 802$ nm and $w_p = 100$ μm).

The characterization of the thermal lensing in the 1.8 at.% $Tm:Lu_2O_3$ crystal is shown in Fig. 8. With increasing P_{abs}, the divergence of the laser beam decreases indicating a positive, focusing TL effect, see Fig. 8(a). The corresponding optical

power D of the TL is plotted in Fig. 8(b). The dependence of D on P_{abs} is close to linear. Its slope is called the sensitivity factor [44]:

$$M = \frac{dD}{dP_{abs}}. \quad (3)$$

In Fig. 8(b), we also show the input-output dependence of the 1.8 at.% Tm:Lu_2O_3 laser.

In Table IV, we have listed the M-factors, the corresponding laser wavelengths λ_L and the root mean square (rms) pump spot radii in the crystal $\langle w_p \rangle$ for the cubic Tm:RE_2O_3 crystals. Here, $\langle w_p \rangle$ is averaged geometrically and does not account for the absorption coefficient. The thermal lens is positive (focusing) in all three Tm:RE_2O_3 crystals. Tm:Lu_2O_3 shows the lowest sensitivity factor.

TABLE IV
SENSITIVITY FACTORS OF THERMAL LENS IN Tm^{3+}-DOPED CUBIC SESQUIOXIDE CRYSTALS

Crystal	Doping	M, m^{-1}/W	$\langle w_p \rangle$, μm	λ_L, nm
Tm:Y_2O_3	2.5 at.%	6.9	116	2055
Tm:Lu_2O_3	1.8 at.%	3.5	133	2070
Tm:Sc_2O_3	2.0 at.%	8.3	112	1995

B. Fractional Heat Load

The fractional heat load η_h is an important parameter for laser materials. It determines the part of the absorbed pump power dissipated as heat, $\eta_h = P_{heat}/P_{abs}$. The η_h value for the 2.5 at.% Tm:Y_2O_3, 1.8 at.% Tm:Lu_2O_3 and 2.0 at.% Tm:Sc_2O_3 crystals was determined by an ISO-standard laser calorimetry (pulsed method) which is based on the analysis of the heating and cooling rates of a thermally isolated material [45]. The measurements were carried out under non-lasing conditions.

As an example, Fig. 9 shows the evaluation of η_h for the 2.5 at.% Tm:Y_2O_3 and 1.8 at.% Tm:Lu_2O_3 samples pumped at λ_p = 802 nm. η_h was calculated as [45]:

$$\eta_h = \frac{T_p m C}{t_p P_{abs}}, \quad (4)$$

where t_p is the duration of the pump pulse, T_p is the temperature at the time $t_p/2$ extrapolated from the cooling curve, and m and C are the mass and specific heat of the crystal, respectively. The calculation of η_h is presented in Table V. η_h is slightly lower for Tm:Lu_2O_3 (0.34±0.05) as compared to Tm:Y_2O_3 and Tm:Sc_2O_3 (0.37±0.05).

Typically, η_h can be estimated as $1 - \eta_{St}$, where η_{St} is the Stokes efficiency determined as $\eta_{St,L} = \lambda_p/\lambda_L$ (under lasing conditions) and $\eta_{St,NL} = \lambda_p/\langle\lambda_{lum}\rangle$ (non-lasing conditions, $\langle\lambda_{lum}\rangle$ is the mean luminescence wavelength). As mentioned in the previous section, the quantum efficiency in Tm^{3+} doped materials is >1 due to cross relaxation. Therefore, the actual laser efficiency can be higher than the Stokes efficiency, resulting in a lower fractional heat load of $\eta_h < 1 - \eta_{St}\eta_q$.

For Tm:Lu_2O_3, $\langle\lambda_{lum}\rangle$ = 1927 nm, which yields $\eta_{St,NL}$ = 0.416. With this value and the measured η_h, the quantum efficiency η_q can be estimated to be at most 1.59. This is lower than the value obtained from the spectroscopic data, η_q = 1.91, cf. Fig. 6(b), indicating parasitic processes (ETU and ESA) at the high inversion densities under non-lasing conditions.

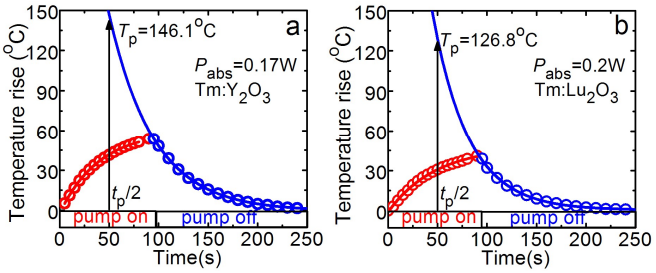

Fig. 9. Evaluation of the fractional heat load η_h in (a) 2.5 at.% Tm:Y_2O_3 and (b) 1.8 at.% Tm:Lu_2O_3 crystals by an ISO-standard laser calorimetry (pulsed method), *red and blue circles* – measured temperature rise in the crystal when the pump is on ($t = 0...t_p$) and off ($t > t_p$), respectively, *solid curves* – exponential fits. T_p is the temperature at the moment $t = t_p/2$ extrapolated from the cooling curve.

TABLE V
EVALUATION OF THE FRACTIONAL HEAT LOAD IN Tm^{3+}-DOPED SESQUIOXIDE CRYSTALS

Crystal	Doping	P_{abs}, W	m, g	C, J/gK	t_p, s	T_p, °C	η_h
Tm:Y_2O_3	2.5 at.%	0.17	0.0814	0.457	90	146.1	0.37
Tm:Lu_2O_3	1.8 at.%	0.24	0.2407	0.24	90	126.8	0.34
Tm:Sc_2O_3	2.0 at.%	0.21	0.0771	0.70	90	108.9	0.37

C. Thermo-Optic Coefficients

The simultaneous measurement of the sensitivity factor M of the thermal lens and the fractional heat load η_h allowed us to evaluate relevant thermo-optic parameters of the cubic Tm:RE_2O_3 crystals from the following formula [46]:

$$M = \frac{\eta_h}{2\pi\langle w_p \rangle^2 \kappa}\chi, \quad (5)$$

where $\langle w_p \rangle$ is the rms pump spot radius in the crystal, κ is the thermal conductivity, and χ is the so-called "generalized" thermo-optic coefficient (TOC) [44]. For cubic crystals, the latter can be approximated as [46]:

$$\chi = dn/dT + (1+\nu)(n-1)\alpha, \quad (6)$$

where dn/dT is the TOC under zero strain, ν is the Poisson ratio, n is the refractive index, and α is the thermal expansion coefficient. In Eq. (6), the two terms represent the temperature dependence of the refractive index (dn/dT) and macroscopic end-bulging of the crystal surfaces due to non-uniform thermal expansion ($Q_{dist} = (1 + \nu)(n - 1)\alpha$), respectively. The third possible effect, namely the photo-elastic term (P_{PE}), is omitted in Eq. (6) as it is typically small for cubic crystals [46].

TABLE VI
EVALUATION OF THERMO-OPTIC PARAMETERS OF Tm^{3+}-DOPED SESQUIOXIDE CRYSTALS AT ~2 μm

Crystal	κ, [2] W/mK	χ, 10^{-6} K^{-1}	α, 10^{-6} K^{-1}	ν	n [51]	dn/dT, 10^{-6} K^{-1}
Tm:Y_2O_3	8.6	13.6	6.56 [13]	0.30 [48]	1.873	6.1
Tm:Lu_2O_3	12.3	13.9	5.88 [14]	0.29 [49]	1.895	7.1
Tm:Sc_2O_3	8.2	14.5	6.3 [47]	0.29 [50]	1.946	6.8

The results on the thermo-optic parameters (χ and dn/dT) for the cubic Tm:RE_2O_3 crystals are shown in Table VI. An important conclusion is that all studied Tm:RE_2O_3 crystals are characterized by a positive dn/dT coefficient (6...7×10^{-6} K^{-1}) which slightly decreases in the sequence RE = Lu – Sc – Y.

In Table VII, we have compared the dn/dT coefficients for cubic RE_2O_3 crystals and ceramics reported so far. Our data are in good agreement with the direct measurements from [51] taking into account the dispersion of the TOCs. The negative sign of the dn/dT coefficient for Sc_2O_3 ceramics reported in [47] (taking into account the similarity of TOCs for crystals and ceramics [47]) is not confirmed in the present work.

TABLE VII
THERMO-OPTIC COEFFICIENTS OF SESQUIOXIDE CRYSTALS AND CERAMICS REPORTED SO FAR

Material	Form	dn/dT, 10^{-6} K^{-1}	λ, μm	Method*	Ref.
Y_2O_3	crystal	6.1	2.06	TL	**
	crystal	6.6	1.1	MD	[51]
	ceramics	5.5	1.06	IF	[52]
	ceramics	8.3	0.63	IF	[53]
	ceramics	8.1	0.63	IF	[47]
Lu_2O_3	crystal	7.1	2.07	TL	**
	crystal	5.8	1.03	TG	[14]
	crystal	7.6	1.1	MD	[51]
	ceramics	8.2	0.63	TG	[47]
Sc_2O_3	crystal	6.8	2.00	TL	**
	crystal	6.9	1.1	MD	[51]
	ceramics	-21.5	0.63	IF	[47]

*TL – thermal lens study, MD – minimum deviation, IF – interferometry, TG – thermal gradient method. **This work.

The positive thermal lens in cubic Tm:RE_2O_3 crystals enables laser operation of these materials in a plano-plano laser cavity, i.e., microchip Tm:RE_2O_3 lasers can be realized. A "cold" plano-plano cavity, meaning an unpumped crystal, is unstable. Pumping a laser crystal characterized by $D > 0$ (and, accordingly, $\chi > 0$) leads to an increase of the total optical path length in the pumped volume [35] with respect to the surrounding regions. This effect provides mode confinement (thermal guiding) in the resonator [34,54].

IV. MICROCHIP TM^{3+}:RE_2O_3 LASERS

A. Laser Set-up

At first, we studied microchip laser operation with the four crystals of Table I in the laser set-up shown in Fig. 10. The crystal dimensions (thickness and aperture) are listed in Table VIII.

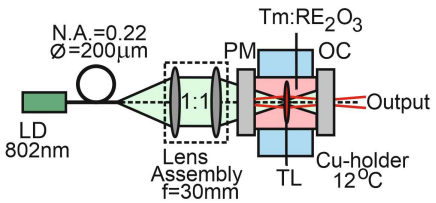

Fig. 10. Scheme of Tm:RE_2O_3 microchip lasers: LD – laser diode, PM – pump mirror, OC – output coupler, TL – thermal lens.

The laser cavity consisted of a flat pump mirror coated for HT at 0.8 μm and HR at 1.8-2.1 μm and different flat output couplers with transmission between 1.5% and 9% in the laser wavelength range of 1.8-2.1 μm. The crystal holder described in Section III A was used. Both surfaces of the laser crystal were polished to laser-grade quality and remained uncoated.

TABLE VIII
ACTIVE ELEMENTS FROM TM^{3+}-DOPED CUBIC SESQUIOXIDE CRYSTALS

Crystal	Doping	t, mm	Aperture, mm^2	η_{abs}, %
Tm:Y_2O_3	2.5 at.%	3.03	2.72×3.10	33
Tm:Lu_2O_3	1.8 at.%	1.73	1.92×3.02	28
	4.0 at.%	2.28	2.62×2.72	36
Tm:Sc_2O_3	2.0 at.%	2.18	3.08×3.11	20

The pump and output coupling mirrors were placed close to the crystal, so the cavity length was close to its thickness. The crystal was pumped by the same laser diode as for the thermal lens experiments (diode #1, with λ_p = 802 nm, and w_p = 100 μm) using the lens assembly described in in Section III A. The pump waist was in the center of the laser crystal. As all the output couplers provided a partial reflection (~40%) at the pump wavelength, the crystal was pumped in a double-pass. The pump absorption efficiency η_{abs} is listed in Table VIII.

Stable microchip laser operation was achieved with all four crystals. The laser emission was unpolarized.

B. Laser Performance

The output characteristics of the 2.5 at.% Tm:Y_2O_3, 1.8 at.% Tm:Lu_2O_3 and 2.0 at.% Tm:Sc_2O_3 microchip lasers are shown in Fig. 11(a,c,e).

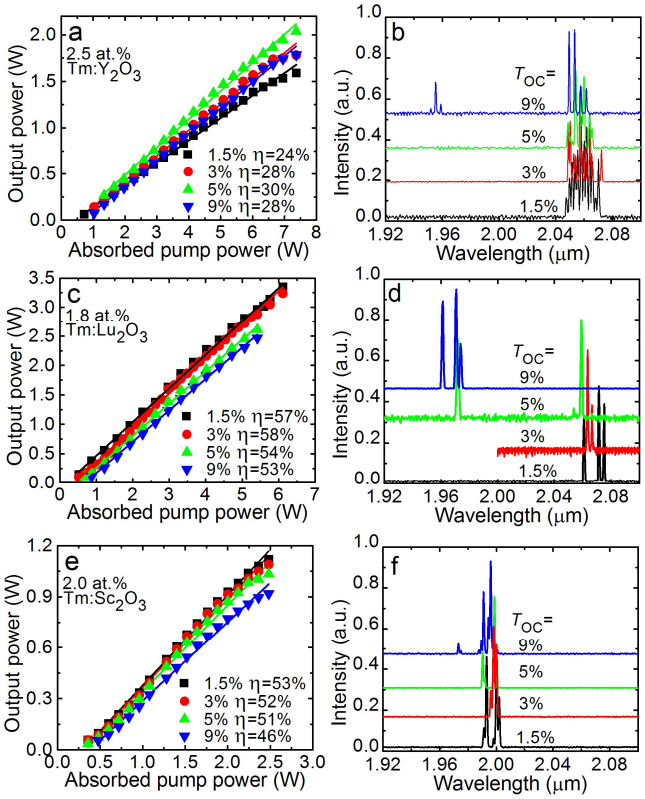

Fig. 11. (a-f) Microchip lasers based on cubic Tm:RE_2O_3 crystals (cf. Table VIII): (a,c,e) input-output dependences (η – slope efficiency) and (b,d,f) typical laser emission spectra (measured at the maximum P_{abs}); λ_p = 802 nm and w_p = 100 μm.

The 1.8 at.% Tm:Lu_2O_3 microchip laser generated an output power of 3.24 W. It operated at wavelengths between 2063 and 2066 nm with a slope efficiency of η = 58% (*vs.* P_{abs}) for T_{OC} = 3%, Fig. 11(c). The laser threshold was at P_{th} = 0.41 W. No thermal roll-over or crystal damage were observed up to the maximum absorbed pump power of 6.1 W. For T_{OC} = 1.5%, the laser output was slightly higher, 3.35 W at 2061-2075 nm, at a lower slope efficiency of 57%.

The 2 at.% Tm:Sc_2O_3 microchip laser operated with only slightly lower slope efficiency of 53% (for T_{OC} = 1.5%) while the output power was limited to 1.12 W at 1991-2002 nm due to the lower pump absorption efficiency η_{abs}. The latter is due to a mismatch of the pump wavelength and the peak in the absorption spectrum, and possibly lower average Tm^{3+} doping (see Section V A). For the 2.5 at.% Tm:Y_2O_3, further drop of the laser slope efficiency (η = 30%) was observed and the maximum output power was 2.04 W at 2049-2065 nm (for the best T_{OC} = 5%). The inferior laser performance of the Tm:Y_2O_3 crystals as compared to that of the Tm:Lu_2O_3 and Tm:Sc_2O_3 ones is related to the lower optical quality of yttria crystals, namely the intrinsic scattering centers [30,55].

A deterioration of the laser output at highest T_{OC} was detected for all Tm:RE_2O_3 microchip lasers and attributed to increased upconversion losses (see Section V B). This effect was more evident for Tm:Sc_2O_3 and Tm:Y_2O_3 crystals. It can be explained by the increasing inversion which is needed to compensate for the losses which are introduced by the higher T_{OC}. The higher inversion leads to a higher probability of the ETU process $Tm_1(^3F_4) + Tm_2(^3F_4) \rightarrow Tm_1(^3H_4) + Tm_2(^3H_6)$, counteracting the CR process, see Fig. 1. Thus, the population of the $^3H_4$ manifold is increased and ESA and other ETU processes which terminate in higher-lying manifolds, are enhanced. This effect can be seen from an increasing intensity of the blue (~480 nm) Tm^{3+} upconversion luminescence (UCL), $^1G_4 \rightarrow {}^3H_6$, with the output coupling. Indeed, the $^1G_4$ manifold can only be populated via ESA and ETU processes.

The typical spectra of output laser emission from the 2.5 at.% Tm:Y_2O_3, 1.8 at.% Tm:Lu_2O_3 and 2.0 at.% Tm:Sc_2O_3 microchip lasers are shown in Fig. 11(b,d,f). For all crystals and OCs, multi-peak spectra are observed due to etalon (Fabry-Perot) effects.

The 1.8 at.% Tm:Lu_2O_3 microchip laser operated at 2063–2075 nm for small T_{OC} of 1.5% and 3%, Fig. 11(d). For T_{OC} = 5%, emission at two distinct wavelengths (1972 and 2060 nm) was observed and for T_{OC} = 9%, the laser emitted at 1960–1973 nm. This behavior is well in line with the values expected from the gain spectra, Fig. 5(b). A similar spectral behavior was observed also for the 2.5 at.% Tm:Y_2O_3 laser. For the 2.0 at.% Tm:Sc_2O_3 laser, only emission at ~2 μm was detected and the emission spectra were weakly dependent on T_{OC}.

As expected from the gain spectra in Fig. 5, the laser emission wavelengths experience a red shift in the sequence RE = Y – Lu – Sc, Fig. 11(b,d,f).

The microchip laser performance of the four cubic Tm:RE_2O_3 crystals from Table VIII is compared in Fig. 12. The performance of the 4.0 at.% Tm:Lu_2O_3 crystal was inferior both in terms of the output power and slope efficiency (with a thermal roll-over at P_{abs} > 6.5 W) compared to the 1.8 at.% Tm:Lu_2O_3 crystal. This is attributed to the increasing upconversion losses for higher Tm^{3+}-doping.

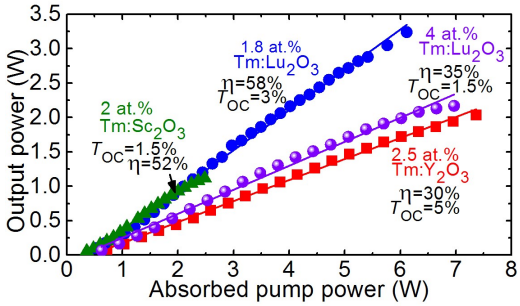

Fig. 12. Comparison of the output performance of the microchip lasers based on cubic Tm:RE_2O_3 crystals (cf. Table VIII): η – slope efficiency, λ_p = 802 nm and w_p = 100 μm.

TABLE IX
COMPARISON OF OUTPUT CHARACTERISTICS OF TM^{3+} SESQUIOXIDE MICROCHIP LASERS*

Crystal	Doping	T_{OC}, %	P_{out}, W	η, %	λ_L, nm	P_{th}, W
Tm:Y_2O_3	2.5 at.%	5	2.04	30	2049-2065	0.44
Tm:Lu_2O_3	1.8 at.%	3	3.24	58	2063-2066	0.41
	4.0 at.%	1.5	2.17	35	2066-2076	0.49
Tm:Sc_2O_3	2.0 at.%	1.5	1.12	53	1991-2002	0.33

*λ_p = 802 nm and w_p = 100 μm. Cf. Table VIII for crystal dimensions.

A summary of the microchip laser parameters of the cubic Tm:RE_2O_3 crystals is presented in Table IX.

The spatial profile of the laser output from the 1.8 at.% Tm:Lu_2O_3 microchip laser was studied in the far-field, see Fig. 13. This laser generated nearly circular TEM_{00} beam with a measured $M^2 < 1.2$.

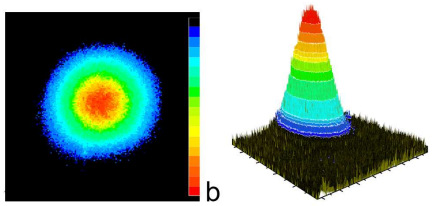

Fig. 13. 2D (a) and 3D (b) profiles of the output laser beam from the Tm:Lu_2O_3 microchip laser, λ_p = 802 nm, P_{abs} = 6.1 W.

C. *Effect of Mode-Matching*

As the best results were obtained with Tm:Lu_2O_3, the further microchip laser studies were performed with this crystal.

The slope efficiency η can be expressed as:

$$\eta < \eta_{mode}\eta_{St,L}\eta_q\eta_{out}, \qquad (7)$$

where η_{mode}, $\eta_{St,L}$ and η_q were defined above and η_{out} is the cavity output-coupling efficiency, the relation of useful losses to total cavity losses, $\eta_{out} = \ln[1-T_{OC}]/\ln[(1-T_{OC})\cdot(1-L)]$ wherein L is the roundtrip passive loss.

Assuming α_{loss} < 0.001 cm^{-1} [30] and η_q = 1.91 (cf. Fig. 6), the mode overlap efficiency of the best 1.8 at.% Tm:Lu_2O_3 laser with η = 58% (see previous section) can be estimated to be in the order of only 80%. To investigate this in more detail, we calculated the radius of the laser mode w_L in the laser crystal. We used the ABCD-formalism and the determined sensitivity factor of the thermal lens, cf. Table IV, as well as the mode overlap efficiency η_{mode} [56]:

$$\eta_{\mathrm{mode}} = \frac{4w_L^2\langle w_p\rangle^2}{(w_L^2+\langle w_p\rangle^2)^2}. \qquad (8)$$

For the considered 1.8 at.% Tm:Lu_2O_3 microchip laser (L_{cav} = 1.73 mm) pumped by the diode #1, the mean pump spot size $\langle w_p\rangle$ = 105 µm. The sensitivity factor of the thermal lens is strongly dependent on $\langle w_p\rangle$, and using Eq. (5) it is calculated to be 5.6 m^{-1}/W. The results on laser mode radius w_L and the overlap efficiency η_{mode} are shown in Fig. 14 vs. the absorbed pump power. Due to the increased optical power at higher pump powers, cf. Eq. (3), the mode radius and thus the overlap efficiency decrease. For a real laser, one needs to account for the variation (typically increase) of the M^2 parameter for the laser mode with the absorbed pump power. This can slightly affect the real η_{mode} value and explain the linear input-output dependences observed in Fig. 11(c) despite the varying η_{mode} in Fig. 14.

The sensitivity of the laser mode diameter in the crystal can be improved by pumping with a smaller pump spot size. For this purpose, we employed a fiber-coupled (fiber core diameter: 105 µm, N.A.: 0.22) AlGaAs LD (diode #2). It emitted up to 30 W of randomly polarized output at λ_p = 792 nm. With the same lens assembly (see Fig. 10) the pump spot radius was reduced to w_p = 52 µm and the confocal parameter accordingly changed to $2z_R$ = 0.90 mm. To enhance the absorption efficiency, we used a longer 1.8 at.% Tm:Lu_2O_3 crystal (t = 5 mm, aperture: 3×3 mm^2). It was polished to laser-grade quality and uncoated. The pump waist was in the center of the laser crystal and $\langle w_p\rangle$ amounted to 98 µm. The same laser set-up as depicted in Fig. 10 was used.

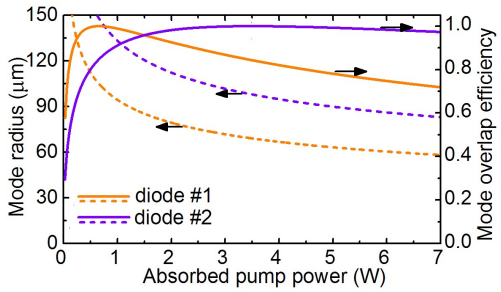

Fig. 14. Mode-matching analysis of the 1.8 at.% Tm:Lu_2O_3 microchip laser: calculated radius of the laser mode w_L and the mode overlap efficiency for the pump and laser beams η_{mode} vs. P_{abs}. *Orange curves*: L_{cav} = 1.73 mm, diode #1 (λ_p = 802 nm, w_p = 100 µm), *violet curves*: L_{cav} = 5.0 mm, diode #2 (λ_p = 791.8 nm, w_p = 52 µm).

The sensitivity factor of the thermal lens for this pump source was estimated to be 6.4 m^{-1}/W. The resulting dependences of w_L and η_{mode} on the pump power are shown in Fig. 14. Also for this set-up, the laser mode radius w_L is strongly reduced to 84 µm, however, the mode overlap efficiency is close to unity within the entire range of applied pump powers.

The input-output characteristics for the 5 mm-thick 1.8 at.% Tm:Lu_2O_3 micro-laser pumped with the diode #2 are shown in Fig. 15(a). The laser emission was unpolarized. This laser generated a maximum output power of 4.89 W at 2058-2070 nm with a maximum slope efficiency of 67% (*vs.* P_{abs}) for T_{OC} = 3%. It should be noted that this value is in good agreement with the value of 69% resulting from Eq. (7). The laser threshold was at 0.29 W. The output dependence was linear up to the highest absorbed pump power of 7.6 W. For T_{OC} of more than 3%, the laser efficiency deteriorated. For T_{OC} > 9%, even a thermal roll-over was observed at P_{abs} > 5.5 W. This is attributed to upconversion losses at the high inversion levels required.

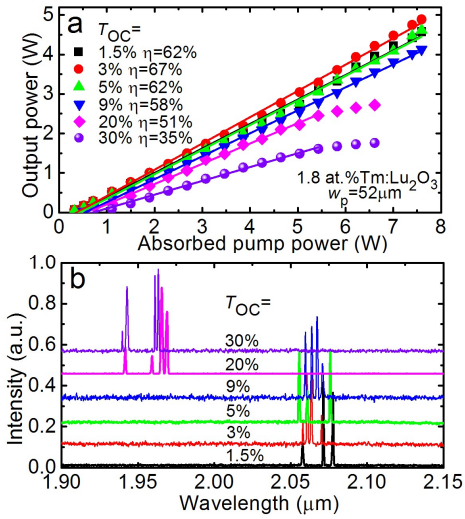

Fig. 15. (a,b) 5 mm-thick 1.8 at.% Tm:Lu_2O_3 micro-laser: (a) input-output dependences, η – slope efficiency; (b) typical laser emission spectra (measured at P_{abs} = 6.6 W); λ_p = 791.8 nm and w_p = 52 µm.

In Fig. 15(b), the typical spectra of laser emission from this laser are presented. For T_{OC} < 10%, the emission is at wavelengths around 2060 nm and for larger T_{OC}, it is observed in two bands at ~1940 and 1960 nm in agreement with the gain spectra, Fig. 5(b).

D. Discussion: Thulium Microchip Lasers

In Table X, we compare the output parameters of the Tm microchip / micro-lasers reported so far. A broad variety of Tm^{3+}-doped crystals has been studied for this type of lasers.

To date, the highest output power from a Tm microchip laser was achieved using a 4 at.% Tm:$YAlO_3$ crystal, namely 6.2 W at a laser wavelength of 2008 nm with η = 46%. The highest slope efficiencies were obtained with monoclinic double tungstate (MDT) crystals: η = 74% for 5 at.% Tm:$KY(WO_4)_2$ (diode-pumping) and η = 77% for 15 at.% Tm:$KLu(WO_4)_2$ (Ti:sapphire laser pumping).

The advantage of Tm^{3+}-doped cubic RE_2O_3 crystals is the possibility to achieve multi-watt laser output with relatively high slope efficiencies at wavelengths well above 2 µm, the longest wavelengths for any Tm microchip laser, see Table X.

For cubic Tm:RE_2O_3 crystals, the absorption cross-sections at ~0.8 µm are moderate (Section II A), and the onset of deterioration of the laser output limits the Tm^{3+} doping concentrations to values below 4 at.% (11.4×10^{20} cm^{-3}) (Section IV B). Nevertheless, it should be noted that this concentration corresponds to 8 at.% in YAG or 18 at.% in $KY(WO_4)_2$ due to the high cation density in Lu_2O_3. Moreover, the thermal and thermo-optic properties are rather advantageous for power scaling, favoring the application of the cubic Tm:RE_2O_3

crystals in compact high-power lasers at >2 μm. Such lasers will be described in Section V.

TABLE X
COMPARISON OF OUTPUT CHARACTERISTICS OF Tm^{3+} MICROCHIP AND MICRO-LASERS REPORTED SO FAR

Crystal	Doping	P_{out}, W	η, %	λ_L, nm	Ref.
$Tm:Y_2O_3$	2.5 at.%	2.04	30	2049-2065	*
$Tm:Lu_2O_3$	1.8 at.%	4.89	67	**2058-2070**	*
$Tm:Sc_2O_3$	2 at.%	1.12	52	1991-2002	*
$Tm:KLu(WO_4)_2$	3 at.%	3.2	50	1946	[54]
	15 at.%	0.79	**77**	1957-1965	[42]
$Tm:KY(WO_4)_2$	5 at.%	2.57	74	1946	[57]
$Tm:MgWO_4$	0.89 at.%	3.09	50	2022-2034	[58]
$Tm:LiYF_4$	8 at.%	3.1	72	1904	[59]
$Tm:LiLuF_4$	12 at.%	2.65	52	1916	[59]
$Tm:LiGdF_4$	8 at.%	1.87	65	1902	[59]
$Tm:YAlO_3$	4 at.%	**6.2**	46	2008	[60]
$Tm:CaGdAlO_4$	3 at.%	1.16	32	1883-1893	[61]
$Tm:Y_3Al_5O_{12}$	10 at.%	0.45	32	2013	[62]
$Tm:YVO_4$	5 at.%	0.40	25	1920	[63]
$Tm:GdVO_4$	6.9 at.%	0.11	47	1950	[64]

*This work.

V. COMPACT HIGH POWER Tm^{3+}:RE_2O_3 LASERS

A. Laser Set-up

A power scaling concept maintaining the high efficiency of compact diode-pumped $Tm:Lu_2O_3$ and $Tm:Sc_2O_3$ lasers was investigated utilizing the plano-plano laser cavity geometry. Its set-up is shown in Fig. 16.

Here, the laser crystal was prepared as a rod (diameter: 3 mm, length: 15 mm). The barrel-polished rod was directly water-cooled to 18 °C. It was pumped by the focused beam of an AlGaAs laser diode emitting up to 140 W at 795-798 nm (spectral bandwidth: 2.7 nm) depending on the output power (diode #3). The diode emission was directly focused into the rod by a f = 80 mm spherical lens resulting in an asymmetric pump spot of 400×750 μm² ($1/e^2$). The barrel polishing was not essential to assure guiding of the pump light, since its beam quality was high enough to pass the laser rod without striking its borders. The flat input mirror was coated for HT at ~0.8 μm and for HR at 1.9-2.2 μm. Different flat output couplers with transmission between 1% and 23% at 1.9-2.1 μm and HT (>90%) at the pump wavelength were tested. For the $Tm:Sc_2O_3$ laser due to the emission at >2.1 μm, for some OCs, the actual transmission at the laser wavelength was higher. The geometrical length of the cavity was ~18 mm. The transmitted pump light was separated from the laser beam by a dichroic plate coated for HR at ~0.8 μm and HT at ~2 μm under an angle of 45°. Thus, direct measurement of the transmitted pump power (and calculation of P_{abs}) was possible under lasing conditions.

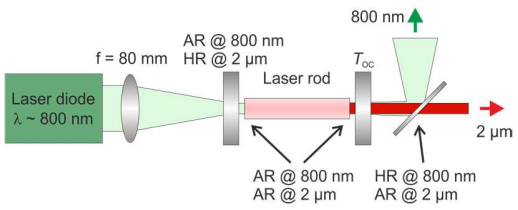

Fig. 16. Scheme of the high-power diode-pumped compact $Tm:Lu_2O_3$ and $Tm:Sc_2O_3$ lasers using a plano-plano laser cavity.

Rods from 1.0 at.% and 1.2 at.% $Tm:Lu_2O_3$, as well as 1.0 at.% and 1.5 at.% $Tm:Sc_2O_3$ crystals were prepared (not listed in Table I). These crystals were grown by the HEM method [37]. Due to less than unity distribution coefficient of Tm^{3+} in Sc_2O_3, a small gradient of the Tm^{3+} concentration was present in the $Tm:Sc_2O_3$ rods. According to the measured absorption spectra, the average doping concentration was $(0.9\ at.\%)_{av}$ and $(1.1\ at.\%)_{av}$, respectively [30].

B. Laser Performance

The best results were achieved for the 1.2 at.% $Tm:Lu_2O_3$ and $(1.1\ at.\%)_{av}$ $Tm:Sc_2O_3$ laser rods. The corresponding input-output dependences are shown in Fig. 17.

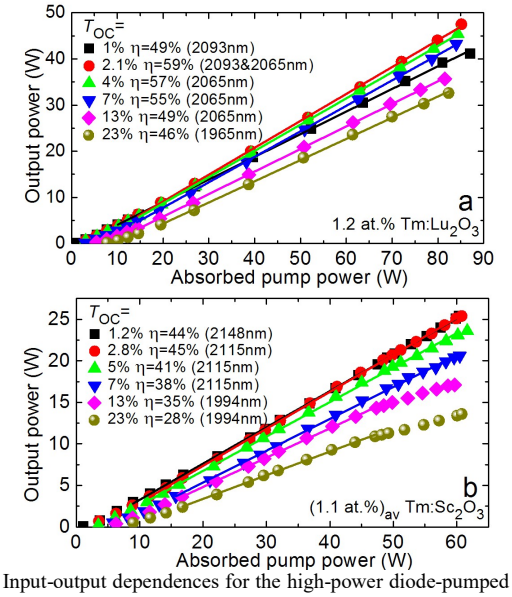

Fig. 17. Input-output dependences for the high-power diode-pumped compact (a) 1.2 at.% $Tm:Lu_2O_3$ and (b) $(1.1\ at.\%)_{av}$ $Tm:Sc_2O_3$ lasers using a plano-plano laser cavity, η – slope efficiency [30].

The 1.2 at.% $Tm:Lu_2O_3$ laser, Fig. 17(a), generated up to 47.5 W at 2065 and 2093 nm at η = 59% (for T_{OC} = 2.1%). The corresponding P_{abs} amounted to 85.1 W, so that the optical-to-optical efficiency η_{opt} reached 56% (*vs.* P_{abs}). At this point, the incident pump power was 122 W. The laser threshold was at 1.9 W in this case. For all OCs, the input-output dependences were clearly linear indicating weak detrimental thermal effects. The wavelength of the laser emission experienced a blue-shift from 2093 nm (T_{OC} = 1%) to 2065 nm (T_{OC} = 4 – 13%) and finally to 1965 nm for T_{OC} = 23%. This agrees with the gain spectra, Fig. 5(b). With output coupler transmissions above 2.1%, the slope efficiency decreased. This behavior is similar to the microchip experiments, Fig. 11.

The $(1.1\ at.\%)_{av}$ $Tm:Sc_2O_3$ laser generated a maximum output power of 25.4 W at 2115 nm with η = 45%, Fig. 17(b). A slight thermal roll-over was observed for P_{abs} > 50 W at high T_{OC}. The highest pump power incident to the $Tm:Sc_2O_3$ laser was limited to 94 W since for higher powers, the temperature drift of the emission wavelength of the diode resulted in strong decrease of the absorption efficiency. The laser thresholds were similar to those for the $Tm:Lu_2O_3$ laser. A similar blue-shift of the emission wavelength with T_{OC} was observed for $Tm:Sc_2O_3$,

however, the laser wavelengths were 2148, 2115 and 1994 nm. The wavelength of 2148 nm is remarkably long for a Tm^{3+}-based CW laser and even longer than the value of 2131 nm achieved recently in a "vibronic" $Tm:KLu(WO_4)_2$ laser [65]. It should be noted that even longer wavelengths up to 2164 nm were obtained with $Tm:Sc_2O_3$ in wavelength tuning experiments [30]. The decrease of the slope efficiency with increasing T_{OC} is more pronounced for $Tm:Sc_2O_3$. ETU processes are more likely to occur in $Tm:Sc_2O_3$ compared to $Tm:Lu_2O_3$ because of the broader spectra and greater overlap of absorption and emission bands, as well as higher cation density, which enhance the ETU probabilities.

In Table XI, we have compared the best output parameters achieved with all four studied laser rods. An increase of Tm^{3+} doping concentration led to a higher slope efficiency for both $Tm:Lu_2O_3$ and $Tm:Sc_2O_3$. This is attributed to more efficient cross relaxation (see Fig. 6(b)). Indeed, the lifetime of the $^3H_4$ pump level for $Tm:Lu_2O_3$ decreases from 83 to 50 µs when the Tm^{3+} concentration is increased from 1 to 1.2 at.% [30].

TABLE XI
COMPARISON OF OUTPUT CHARACTERISTICS OF HIGH-POWER TM^{3+} SESQUIOXIDE LASERS USING A PLANO-PLANO CAVITY

Crystal	Doping	P_{out}, W	η, %	λ_L, nm	η_{abs}, %
$Tm:Lu_2O_3$	1.0 at.%	36.8	56	2065	59-75
	1.2 at.%	47.5	59	2065&2093	67-81
$Tm:Sc_2O_3$	$(0.9\ at.\%)_{av}$	21.3	41	2115	57-75
	$(1.1\ at.\%)_{av}$	25.4	45	2115	63-84

VI. CONCLUSION

We reported on a detailed comparative study of the spectroscopic, thermo-optic and laser properties of three Tm^{3+}-doped cubic sesquioxide crystals, Lu_2O_3, Y_2O_3 and Sc_2O_3, concerning their potential for compact, highly-efficient and power-scalable eye-safe lasers. Tm^{3+} ions in the RE_2O_3 crystals feature large splitting of the ground-state, $^3H_6$, and the upper laser level, $^3F_4$, leading to broadband absorption and emission properties and, in particular, the possibility of laser operation well above 2 µm. Efficient cross relaxation is featured in the $Tm:RE_2O_3$ crystals at Tm^{3+} doping levels of ~2 at.%. A combination of high thermal conductivity, weak thermal expansion and weak and positive thermal lensing arising from positive dn/dT coefficients, opens the possibilities for power scaling of compact $Tm:RE_2O_3$ lasers based on thermal guiding, e.g. in microchip geometry from few watts up to tens of watts of output power at >2 µm. Passive Q-switching of compact $Tm:RE_2O_3$ lasers, e.g. by Cr^{2+}:ZnS or Cr^{2+}:ZnSe crystals or ceramics, is promising because the generation of high-energy pulses will benefit from the relatively long storage time of the $Tm:RE_2O_3$ crystals of ~3.5 ms while short pulse durations will be possible due to the compact cavity design.

REFERENCES

[1] L. Pauling and M. D. Shappell, "The crystal structure of bixbyite and the C-modifications of the sesquioxides," *Z. Kristallogr.*, vol. 75, no. 1, pp. 128-142, Dec. 1930.

[2] C. Kränkel, "Rare-earth-doped sesquioxides for diode-pumped high-power lasers in the 1-, 2-, and 3-µm spectral range," *IEEE J. Sel. Top. Quantum Electron.*, vol. 21, no. 1, pp. 1602013, Jan. 2015.

[3] K. Petermann *et al*., "Rare-earth-doped sesquioxides", J. Lumin., vol. 87-89, pp. 973-975, May 2000.

[4] K. Petermann, L. Fornasiero, E. Mix, and V. Peters, "High melting sesquioxides: crystal growth, spectroscopy, and laser experiments," *Opt. Mater.*, vol. 19, no. 1, pp. 67-71, Feb. 2002.

[5] P. Koopmann, R. Peters, K. Petermann, and G. Huber, "Crystal growth, spectroscopy and highly efficient laser operation of thulium-doped Lu_2O_3 around 2 µm," *Appl. Phys. B, Lasers Opt.*, vol. 102, no. 1, pp. 19–24, Jan. 2011.

[6] P. Koopmann, S. Lamrini, K. Scholle, P. Fuhrberg, K. Petermann, and G. Huber, "Efficient diode-pumped laser operation of $Tm:Lu_2O_3$ around 2 µm," *Opt. Lett.*, vol. 36, no. 6, pp. 948-950, Mar. 2011.

[7] P. Koopmann, S. Lamrini, K. Scholle, M. Schäfer, P. Fuhrberg, and G. Huber, "Holmium-doped Lu_2O_3, Y_2O_3, and Sc_2O_3 for lasers above 2.1 µm," *Opt. Exp.*, vol. 21, no. 3, pp. 3926–3931, Feb. 2013.

[8] P. Koopmann, S. Lamrini, K. Scholle, M. Schäfer, P. Fuhrberg, and G. Huber, "Multi-watt laser operation and laser parameters of Ho-doped Lu_2O_3 at 2.12 µm," *Opt. Mater. Exp.*, vol. 1, no. 8, pp. 1447–1456, Dec. 2011.

[9] P. von Brunn, A. M. Heuer, L. Fornasiero, G. Huber, and C. Kränkel, "Efficient laser operation of $Nd^{3+}:Lu_2O_3$ at various wavelengths between 917 nm and 1463 nm," *Laser Phys*., vol. 26, no. 8, pp. 084003, Aug. 2016.

[10] T. Li, K. Beil, C. Kränkel, and G. Huber, "Efficient high-power continuous wave $Er:Lu_2O_3$ laser at 2.85 µm," *Opt. Lett*., vol. 37, no. 13, pp. 2568–2570, July 2012.

[11] A. Schmidt *et al*., "Diode-pumped mode-locked $Yb:LuScO_3$ single crystal laser with 74 fs pulse duration," *Opt. Lett*., vol. 35, no. 4, pp. 511–513, Feb. 2010.

[12] R. Peters *et al*., "Thermal analysis and efficient high power continuous-wave and mode-locked thin disk laser operation of Yb-doped sesquioxides," *Appl. Phys. B, Lasers Opt.*, vol. 102, no. 3, pp. 509–514, Mar. 2011.

[13] P. H. Klein and W. J. Croft, "Thermal conductivity, diffusivity, and expansion of Y_2O_3, $Y_3Al_5O_{12}$ and LaF_3 in the range 77–300 K," *J. Appl. Phys.*, vol. 38, no. 4, p. 1603-1607, Mar. 1967.

[14] P. A. Loiko *et al*., "Thermo-optic properties of $Yb:Lu_2O_3$ single crystals," *Appl. Phys. B, Lasers Opt.*, vol. 120, no. 4, pp. 601–607, Sep. 2015

[15] R. Peters, C. Kränkel, K. Petermann, and G. Huber, "Crystal growth by the heat exchanger method, spectroscopic characterization and laser operation of high-purity $Yb:Lu_2O_3$," *J. Cryst. Growth*, vol. 310, no. 7, pp. 1934-1938, Apr. 2008.

[16] M. V. Abrashev, N. D. Todorov, and J. Geshev, "Raman spectra of R_2O_3 (R-rare earth) sesquioxides with C-type bixbyite crystal structure: A comparative study," *J. Appl. Phys*., vol. 116, no. 10, pp. 103508, Sept. 2014.

[17] C. R. Stanek, K. J.McClellan, B. P. Uberuaga, K. E. Sickafus, M. R. Levy, and R. W. Grimes, "Determining the site preference of trivalent dopants in bixbyite sesquioxides by atomic-scale simulations," *Phys. Rev. B*, vol. 75, no. 13, pp. 134101, Apr. 2007.

[18] R. Peters, C. Kränkel, K. Petermann, and G. Huber, "Broadly tunable high-power $Yb:Lu_2O_3$ thin disk laser with 80% slope efficiency," *Opt. Exp*., vol. 15, no. 11, pp. 7075–7082, May 2007.

[19] A. A. Lagatsky, O. L. Antipov, and W. Sibbett, "Broadly tunable femtosecond $Tm:Lu_2O_3$ ceramic laser operating around 2070 nm," *Opt. Exp.,* vol. 20, no. 17, pp. 19349–19354, Aug. 2012.

[20] M. Tokurakawa *et al*., "Diode-pumped 65 fs Kerr-lens mode-locked Yb^{3+}: Lu_2O_3 and nondoped Y_2O_3 combined ceramic laser," *Opt. Lett.,* vol. 33, no. 12, pp. 1380-1382, June 2008.

[21] U. Griebner, V. Petrov, K. Petermann, and V. Peters, "Passively mode-locked $Yb:Lu_2O_3$ laser," *Opt. Exp.*, vol. 12, no. 14, pp. 3125-3130 July 2004.

[22] M. Tokurakawa *et al*., "Ultrashort pulse generation from diode pumped mode-locked Yb^{3+}:sesquioxide single crystal lasers," *Opt. Exp.*, vol. 19, no. 4, pp. 2904–2909, Feb. 2011.

[23] A. Schmidt *et al*., "175 fs $Tm:Lu_2O_3$ laser at 2.07 µm mode-locked using single-walled carbon nanotubes," *Opt. Exp*., vol. 20, no. 5, pp. 5313-5318, Feb. 2012.

[24] A. A. Lagatsky, P. Koopmann, P. Fuhrberg, G. Huber, C. Brown, and W. Sibbett, "Passively mode-locked femtosecond $Tm:Sc_2O_3$ laser at 2.1 µm," *Opt. Lett.*, vol. 37, no. 3, pp. 437–439, Feb. 2012.

[25] C. R. E. Baer *et al*., "Femtosecond $Yb:Lu_2O_3$ thin disk laser with 63 W of average power," *Opt. Lett*., vol. 34, no. 18, pp. 2823–2825, Sept. 2009.

[26] S. V. Marchese *et al*., "Efficient femtosecond high power $Yb:Lu_2O_3$ thin disk laser," *Opt. Exp.*, vol. 15, no. 25, pp. 16966-16971, Dec. 2007.

[27] C. R. E. Baer *et al.*, "Femtosecond thin-disk laser with 141 W of average power," *Opt. Lett.*, vol. 35, no. 13, pp. 2302-2304, July 2010.
[28] T. Südmeyer *et al.*, "High power ultrafast thin disk laser oscillators and their potential for sub-100-femtosecond pulse generation," *Appl. Phys. B, Lasers Opt.*, vol. 97, no. 2, pp. 281–295, Oct. 2009.
[29] R. C. Stoneman and L. Esterowitz, "Efficient, broadly tunable, laser-pumped Tm:YAG and Tm:YSGG cw lasers," *Opt. Lett*., vol. 15, no. 9, pp. 486-488, May 1990.
[30] P. Koopmann, "Thulium- and holmium-doped sesquioxides for 2 µm lasers", Ph.D. Thesis, Dept. Physik, Universität Hamburg, 2012.
[31] K. van Dalfsen, S. Aravazhi, C. Grivas, S. M. García-Blanco, and M. Pollnau, "Thulium channel waveguide laser with 1.6 W of output power and ~80% slope efficiency," *Opt. Lett*., vol. 39, no. 15, pp. 4380-4383, Aug. 2014.
[32] O. L. Antipov, A. A. Novikov, N. G. Zakharov, and A. P. Zinov'ev, "Optical properties and efficient laser oscillation at 2066 nm of novel Tm:Lu_2O_3 ceramics," *Opt. Mater. Exp.*, vol. 2, no. 2, pp. 183–189, Feb. 2012.
[33] A. A. Lagatsky, O. L. Antipov, and W. Sibbett, "Broadly tunable femtosecond Tm:Lu_2O_3 ceramic laser operating around 2070 nm," *Opt. Exp.*, vol. 20, no. 17, pp. 19349–19354, Aug. 2012.
[34] J. J. Zayhowski, "Thermal guiding in microchip lasers," in *Advanced Solid State Lasers*, G. Dube, Ed., Vol. 6 of OSA Proceedings Series (Optical Society of America, 1990), p. DPL3.
[35] J. J. Zayhowski, "Microchip lasers," *Opt. Mater*., vol. 11, pp. 255–267, Jan. 1999.
[36] J. J. Zayhowski and C. Dill, III, "Diode-pumped passively Q-switched picosecond microchip lasers," *Opt. Lett*., vol. 19, no. 18, pp. 1427–1429, Sept. 1994.
[37] F. Schmid and D. Viechnic, "Growth of sapphire disks from melt by a gradient furnace technique," *J. Amer. Ceram. Soc*., vol. 53, no. 9, pp. 528–529, Sept. 1970.
[38] L. Fornasiero, "Nd^{3+} - und Tm^{3+} -dotierte Sesquioxide," Ph.D. Thesis, Dept. Physik, Universität Hamburg, 1999.
[39] B. Aull, and H. Jenssen, "Vibronic interactions in Nd:YAG resulting in nonreciprocity of absorption and stimulated emission cross sections," *IEEE J. Quantum Electron*., vol. 18, no. 5, pp. 925-930, May 1982.
[40] L. Laversenne, Y. Guyot, C. Goutaudier, M. T. Cohen-Adad, and G. Boulon, "Optimization of spectroscopic properties of Yb^{3+}-doped refractory sesquioxides: cubic Y_2O_3, Lu_2O_3 and monoclinic Gd_2O_3," *Opt. Mater.*, vol. 16, no. 4, pp. 475-483, May 2011.
[41] P. Loiko, and M. Pollnau, "Stochastic model of energy-transfer processes among rare-earth ions. Example of Al_2O_3:Tm^{3+}," *J. Phys. Chem. C*, vol. 120, no. 46, pp. 26480-26489, Nov. 2016.
[42] X. Mateos *et al*., "Efficient micro-lasers based on highly-doped monoclinic double tungstates," *IEEE J. Quantum Electron*., vol. 53, no. 3, pp. 1700110-1-10, June 2017.
[43] P. Loiko *et al*., "Thermal lensing and multi-watt microchip laser operation of Yb:YCOB crystals," *IEEE Photonics J*., vol. 8, no. 3, pp. 1501312, June 2016.
[44] P. Loiko, F. Druon, P. Georges, B. Viana, and K. Yumashev, "Thermo-optic characterization of Yb:$CaGdAlO_4$ laser crystal," *Opt. Mater. Exp.*, vol. 4, no. 11, pp. 2241-2249, Nov. 2014.
[45] U. Willamowski, D. Ristau, and E. Welsch, "Measuring the absolute absorptance of optical laser components," *Appl. Opt*., vol. 37, no. 36, pp. 8362-8370, Dec. 1998.
[46] S. Chénais, F. Druon, S. Forget, F. Balembois, and P. Georges, "On thermal effects in solid-state lasers: The case of ytterbium-doped materials," *Prog. Quantum Electron*., vol. 30, no. 4, pp. 89–153, 2006.
[47] V. Cardinali, E. Marmois, B. Le Garrec, and G. Bourdet, "Determination of the thermo-optic coefficient dn/dT of ytterbium doped ceramics (Sc_2O_3, Y_2O_3, Lu_2O_3, YAG), crystals (YAG, CaF_2) and neodymium doped phosphate glass at cryogenic temperature," *Opt. Mater*., vol. 34, no. 6, pp. 990-994, Apr. 2012.
[48] M. J. Weber, "Handbook of Optical Materials," CRC Press, New York, 2003.
[49] W. R. Manning, and O. Hunter, " Elastic properties of polycrystalline thulium oxide and lutetium oxide from 20 to 1000 C," *J. Amer. Ceram. Soc*., vol. 53, no. 5, pp. 279-280, May 1980.
[50] S. Barzilai, I. Halevy, and O. Yeheskel, "Bulk modulus of Sc_2O_3: Ab initio calculations and experimental results," *J. Appl. Phys*., vol. 110, no. 4, pp. 043532, Aug. 2011.
[51] D. E. Zelmon, J. M. Northridge, N. D. Haynes, D. Perlov, and K. Petermann, "Temperature-dependent Sellmeier equations for rare-earth sesquioxides," *Appl. Opt*., vol. 52, no. 16, pp. 3824-3828, June 2013.
[52] T. Y. Fan, "Cryogenic Yb^{3+} doped solid state lasers," *IEEE J. Sel. Top. Quantum Electron*., vol. 13, no. 3, pp. 448-459, May-June 2007.
[53] C. H. Lange, and D. D. Duncan, "Temperature coefficient of refractive index for candidate optical windows," *Proc. SPIE*, vol. 1326, pp. 71–78, Oct. 1990.
[54] J. M. Serres *et al*., "Diode-pumped microchip Tm:$KLu(WO_4)_2$ laser with more than 3 W of output power," *Opt. Lett*., 39, no. 14, pp. 4247-4250, July 2014.
[55] K. Schenk, R. Peters, K. Petermann, and G. Huber, "Investigation of the scattering properties of Yb:Y_2O_3 and its effect on laser parameters," *in CLEO/Europe and EQEC 2009* (Optical Society of America, 2009), p. CA_P20.
[56] Y. F. Chen, T. S. Liao, C. F. Kao, T. M. Huang, K. H. Lin, and S. C. Wang, "Optimization of fiber-coupled laser-diode end-pumped lasers: influence of pump-beam quality," *IEEE J. Quantum Electron*., vol. 32, no. 11, pp. 2010-2016, Nov. 1996.
[57] M. Gaponenko, N. Kuleshov, and T. Sudmeyer, "Passively Q-switched thulium microchip laser," *IEEE Photon. Technol. Lett.*, vol. 28, no. 2, pp. 147–150, Jan. 2016.
[58] P. Loiko *et al*., "Monoclinic Tm^{3+}:$MgWO_4$: a primising crystal for continuous-wave and passively Q-switched lasers at ~2 µm," *Opt. Lett*., vol. 42, no. 6, pp. 1177-1180, Mar. 2017.
[59] P. Loiko *et al*., "Comparative spectroscopic and thermo-optic study of Tm:Li$Ln$$F_4$ (Ln = Y, Gd, and Lu) crystals for highly-efficient microchip lasers at ~2 µm," *Opt. Mater. Exp.*, vol. 7, no. 3, pp. 844-854, Mar. 2017.
[60] J. Šulc, H. Jelínková, K. Nejezchleb, and V. Škoda, "High-efficient room-temperature CW operating Tm:YAP laser with microchip resonator," *Proc. SPIE*, vol. 7193, pp. 71932H, Feb. 2009.
[61] P. Loiko *et al*., "Tm:$CaGdAlO_4$: spectroscopy, microchip laser and passive Q-switching by carbon nanostructures," *Proc. SPIE*, vol. 10082, pp. 1008228, Feb. 2017.
[62] F. F. Heine, and G. Huber, "Tunable single frequency thulium:YAG microchip laser with external feedback," *Appl. Opt*., vol. 37, no. 15, pp. 3268-3271, May 1998.
[63] J. J. Zayhowski, J. Harrison, C. Dill, and J. Ochoa, "Tm:YVO_4 microchip laser," *Appl. Opt*., vol. 34, no. 3, pp. 435–437, Jan. 1995.
[64] C. P. Wyss *et al*., "Emission properties of a Tm^{3+}:$GdVO_4$ microchip laser at 1.9 µm," *Appl. Phys. B, Lasers Opt.*, vol. 67, no. 5, pp. 545–548, Nov. 1998.
[65] P. Loiko *et al*., "Vibronic thulium laser at 2131 nm Q-switched by single-walled carbon nanotubes," *J. Opt. Soc. Amer. B, Opt. Phys.,* vol. 33, no. 11, pp. D19–D27, Nov. 2016.

Pavel Loiko was born in Minsk, Belarus, in 1988. He received the Ph.D. degree in optics from Belarusian State University, Minsk, in 2012.

He was a Researcher with Center for Optical Materials and Technologies (COMT), BNTU, Minsk, in 2013-2015, and a PostDoc with KTH – Royal Institute of Technology, Stockholm, Sweden, in 2015-2016. He is currently a Senior Researcher with ITMO University, Saint Petersburg, Russia. His research interests include spectroscopic, structural, thermo-optic and laser properties of oxide and fluoride crystals and ceramics for applications in bulk and waveguide solid-state lasers.

Philipp Koopmann received his diploma and Ph.D. degrees in physics from the University of Hamburg, Germany in 2009 and 2012, respectively. His research at the Institute of Laser-Physics focused on thulium- and holmium-doped sesquioxides for the generation of 2 µm laser radiation, encompassing crystal growth, spectroscopic characterization, and laser operation.

Since 2013, he is with Alltec GmbH, Germany, working on the application of lasers in material marking.

Xavier Mateos was born in Tarragona, Spain. He received the Ph.D. degree in chemistry from Universitat Rovira i Virgili, Tarragona, in 2004.

He was a Visiting Post-Doctoral Researcher with the Max Born Institute for Nonlinear Optics and Ultrafast Spectroscopy, Berlin, Germany, with a focus on new laser materials for two years. In 2007, he joined the Universitat Rovira i Virgili, where he is currently an Associate Professor. His research interest is the development of new solid-state laser materials operating in the infrared.

Josep Maria Serres was born in Tortosa, Spain. He received the M. Sc. degree in nanoscience and nanotechnology from Universitat Rovira i Virgili, Tarragona, Spain, in 2013, where he is currently pursuing the Ph.D. degree, with a focus on continuous-wave and passively Q-switched microchip lasers in the near-infrared.

Venkatesan Jambunathan received his PhD degree from Universitat Rovira i Virgili, Tarragona, Spain in 2011.

He is currently working as a senior researcher at HiLASE Center, Institute of Physics, Academy of Sciences of the Czech Republic. His research activities include development of solid-state laser materials. Presently his research activity is focused on spectroscopy and laser operation of solid-state laser materials at cryogenic temperatures.

Antonio Lucianetti received his Ph.D. in physics from the University of Bern, Switzerland, in 1999.

He is currently a Group Leader in the HiLASE Centre at the Institute of Physics, Academy of Sciences of the Czech Republic. His research interests include high-energy cryogenic short pulse lasers, microchip lasers, high-energy optical isolators, laser-driven particle and radiation sources, and laser-based interferometric gravitational wave detectors.

Tomas Mocek was born in Prague, Czech Republic, in 1970. He received his Ph.D. degree in physics from the Korea Advanced Institute of Science and Technology (KAIST), South Korea, and in applied physics from the Czech Technical University in Prague, Czech Republic.

He is currently the Head of HiLASE Centre at the Institute of Physics. His research expertise includes development of high average power diode-pumped solid state lasers for hi-tech applications, EUV generation, high-order harmonic generation, mid-IR generation, laser induced periodic surface structures, laser acceleration of particles, dense plasma diagnostics, optical-field ionization, X-ray lasers, and spectroscopy of laser plasma.

Magdalena Aguiló was born in Sa Pobla, Mallorca, Spain. She received the Ph.D. degree in physics from Barcelona University, Barcelona, Spain.

She is currently a Professor of Crystallography, Universitat Rovira i Virgili, Tarragona, Spain. Her research interests include crystal growth, X-ray diffraction, X-ray texture analysis, and physical properties related to the crystalline structure.

Francesc Díaz was born in Lugo, Spain. He received the Ph.D. degree in physics from Barcelona University, Barcelona, Spain.

He is currently a Professor of Applied Physics with Universitat Rovira i Virgili, Tarragona, Spain. His research interests include nanostructuring of optical materials, spectroscopy of rare-earth ions for laser applications, and nonlinear optical processes.

Uwe Griebner received the Ph.D. degree in physics from the Technical University of Berlin, Germany, in 1996, with a focus on fiber bundle lasers with high-average power. Since 1992, he has been with the Max Born Institute for Nonlinear Optics and Short Pulse Spectroscopy, Berlin, where he is currently involved in diode pumped solid-state lasers, fiber lasers, waveguide lasers, ultrafast lasers, and digital holography. He is currently focused on ultrafast diode-pumped semiconductor and solid-state lasers.

Valentin Petrov was born in Plovdiv, Bulgaria, in 1959. He received the M.Sc. degree in nuclear physics from the University of Sofia, Bulgaria, in 1983, and the Ph.D. degree in optical physics from Friedrich-Schiller-University, Jena, Germany, in 1988.

He was an Assistant Professor with the Quantum Electronics Department, Faculty of Physics, University of Sofia, from 1988 to 1991. He was Visiting Post-Doctoral Researcher with the University of Regensburg, Germany, for one year. He joined the Max-Born-Institute for Nonlinear Optics and Ultrafast Spectroscopy, Berlin, Germany, in 1992. His research interests include ultrashort light pulses, laser physics, nonlinear optics, and optical materials. He has co-authored over 460 papers in peer-reviewed scientific journals and over 500 conference presentations. Among the international projects coordinated, he has led two EU consortia within the sixth and seventh Framework Programs.

Dr. Petrov is a member of the Optical Society of America. He served on the committees of few major international conferences, including the CLEO, the ASSL-ASSP, the Europhoton, and the Ultrafast Optics. He is a Regular Reviewer of several international optical journals and a Topical Editor (Lasers) in Optics Letters.

Christian Kränkel studied physics and did his PhD-thesis in the research group of Prof. Günter Huber at the Institut für Laser-Physik (ILP) of the Universität Hamburg, Germany. He spent two years as a Postdoctoral Researcher in the group of Prof. Ursula Keller at the ETH Zurich, Switzerland. Since 2010 he was a Junior Research Group Leader at the ILP and achieved his habilitation degree in February 2017. Since March 2017 he is the leader of the newly installed Zentrum für Lasermaterialien - Kristalle (ZLM) at the Leibniz-Institut für Kristallzüchtung in Berlin, Germany. His research focus lies on the growth of novel ion-doped laser crystals as well as their spectroscopic and laser characterization.